

Study on corrosion and delamination behavior of X70 steel under the coupling action of AC-DC interference and Stress

Xinhua Wang, Xuting Song, Yingchun Chen*, Zuquan Wang, Liuwei Zhang

College of Mechanical Engineering and Applied Electronics Technology, Beijing University of Technology, Beijing 100124, China

*E-mail: ychen08089@163.com

Received: 27 August 2018 / Accepted: 8 November 2018 / Published: 5 January 2019

The combined influences of AC-DC interference and stress on the corrosion and delamination behavior of X70 steel in the neutral environment was studied using COMSOL Multiphysics software, electrochemical tests, weight loss experiments, and surface analysis techniques. Results showed that, under the stress of 364 MPa, as the stray current density increased, the corrosion potential shifted towards the negative side, with no passive region on polarization curves, but only an active dissolution region. Under the influence of DC interference, the anodic polarization curves showed a significant inflection point, due to the accumulation of a large number of corrosion products on the surface of X70 steel, which hindered the anodic polarization. At the same time, the corrosion rate and the maximum depth of the corrosion pits increased with increase in DC density. The corrosion reaction followed Faraday's law of electrolysis. Under the influence of combined AC and DC interferences, the corrosion rate and the depth of the corrosion pits were in the following order: combined AC and DC interferences > DC interference > AC interference. The influence of AC interference on the delamination was less than that of DC interference. The delamination area of the anticorrosive coating under DC interference with a current density of 300 A/m² was about 5 times that under AC interference. Also, under the combined influence of AC and DC interference, the delamination area of the coating was larger than that under the influence of either AC or DC interference. In this paper, a model for delamination process under the influence of stray current was proposed, in which, the corrosion reaction occurred first at the sample defects. When the amount of corrosion product accumulated to a certain extent, separate cathode and anode regions were formed on the sample surface, which resulted in delamination of the coating.

Keywords: AC-DC interference; stray current; stress; corrosion; delamination

1. INTRODUCTION

With rapid developments in electric power, energy, and transportation industries in our country, there has been an increase in the number of buried steel pipelines and high voltage transmission lines or

electrified railways laid, either parallel or intersecting. Concentration of these in a local area forms the “public corridor.” The corrosion of pipeline steel due to the interference of stray current becomes more significant as time passes [1-5]. Leakage in the pipeline causes substantial economic losses and is a potential safety hazard. Stray current interference can be AC, DC, or ground stray current depending on the source. Amongst these, corrosion problem due ground stray current is negligible [6-8], due to improvised insulation coatings of the modern buried pipelines. The stray current in the pipeline can be transmitted through long-distances and then flows out from the defects in the coating, due to damage and spalling, resulting in tremendous local corrosion rate. For example, after laying one X42 pipeline steel coated with fused epoxy powder (FBE) and high voltage (500 KV) AC power parallel transmission wires for one year, the corrosion rate was as high as 10 mm/a [9]. Usually the three-layer polyethylene (3PE) coating of pipeline undergoes delamination, due to stray current disturbances after the pipeline is operational. Once the bonding between the pipeline and coating is lost, the shielding effect of cathodic protection leads to a series of problems, such as pitting corrosion and stress corrosion, which seriously affect the safe operation of the pipelines [10].

Recently, some experts and scholars have carried out some researches to solve the problems of corrosion due to stray current and have achieved some success [11-15]. DC interference has a significant influence on the corrosion of buried steel pipelines, and its essence is the electrolytic effect of electrochemical corrosion [16]. Bertolini, Carsana, and Pedeferrri [17] showed that corrosion could occur in the enhancement phase of the anode region only after the DC has been applied for a certain period. The corrosion amount was related to the current density of the anode, the chloride content in the concrete, and the action of DC. Wang and Tang [18] studied the corrosion behavior of X65 steel under the combined action of DC interference and stress. They found that an increase in the corrosion rate of X65 steel was proportional to the increase in DC density. According to Song, Kim, and Yong [19] the three main factors affecting AC corrosion are AC voltage, AC frequency, and AC density. Goidanich, Lazzari, and Ormellese [20] confirmed experimentally that at an AC density of 10 A/m², corrosion rate of the electrode was twice than that without AC interference. Fu and Cheng [21] found that when the AC density was in the range of 0 ~ 20 A/m², the impact of AC on corrosion of pipeline steel was negligible. They also found that, when the current density was between 20 ~ 100 A/m², corrosion on the pipeline surface was uniform. However, in the range of 100 ~ 500 A/m², the surface of pipeline steel showed characteristic pitting corrosion. Guo [22] studied the effect of AC corrosion on the high-strength pipeline steel by weight loss method. Results showed that the corrosion rate increased with increase in AC density, and decreased with increase in AC interference frequency. Wang [23] studied the effect of AC interference on the delamination behavior of anticorrosive epoxy coatings. Results showed that smaller the defect area of the anticorrosive layer, the larger is the delamination area of the coating when same AC density is applied. AC corrosion process is thus more complicated than DC corrosion process. There are many of corrosion mechanisms such as Faraday rectification [24,25], depolarization of the anode reaction [26], irreversibility of the anodic reaction [27], and oscillation effect of AC voltage at the metal/dielectric interface [28,29]. However, the corrosion mechanisms of the AC corrosion phenomena have limitations.

In the process of conveying high-pressure medium, the high-strength steel pipe is inevitably under stress, which significantly impacts the thermodynamics and kinetics of corrosion of high-strength

steel pipe. Study and exploration of the corrosion problem of high strength steel under stress has become a new topic of research [30]. Under AC and DC interferences, the corrosion of high strength pipeline steel and the delamination behavior of the coating are complex, and the corrosion mechanism is not precise. Therefore, it is important to investigate the corrosion and coating detachment under the combined influence of AC-DC interference and stress.

In this paper, the combined influences of AC-DC interference and stress on corrosion and delamination behavior of X70 steel at the 3PE coating damaged site were studied through open circuit potential tests, polarization curve analysis, and three-dimensional volumetric microscope observation.

2. EXPERIMENTAL

2.1 Materials and test solution

X70 steel pipeline was chosen for the experiment. Its chemical composition (wt%) was C (0.061), Si (0.24), Mn (1.53), P (0.011), S (0.0009), and Fe. The yield stress of X70 steel was 520 MPa. The samples were cut along the axis of the pipe using a wire cutting machine, the sample size of which is shown in Fig.1. Fig. 2 shows the von Mises stress distribution on the surface of the samples upon application of 364 MPa tensile stress, which is 70% yield stress of the X70 pipeline steel. It is evident that the stresses at the fillet transition zone and the stress point of the samples were the largest, whereas the stresses in other regions were even. Thus, the chosen experimental sample sizes met the requirements. After being polished by 60 #, 400 #, and 800 # waterproof sandpapers sequentially, the working specimen showed a mirror-like metal surface with no scratches. The samples were washed with acetone, deionized water, and absolute ethanol successively. Thereafter, they were dried; the non-working surfaces of the samples were sealed with silica gel, and then brushed with 3PE cold-wound belt matching primer on the working surface. It was ensured that all the parallel samples had consistent thicknesses and physical properties during brushing. After the primer surface was dried, the coatings were made according to the requirements of 3PE construction tape. A $2 \times 2 \text{ mm}^2$ damage point in the middle of the 3PE coating was made to simulate the inflow point and outflow point of stray current. NaCl solution, with a mass fraction of 3.5%, was used as the electrolyte solution. The samples were divided into three parallel groups for electrochemical test, corrosion rate measurement, and observation of corrosion morphologies.

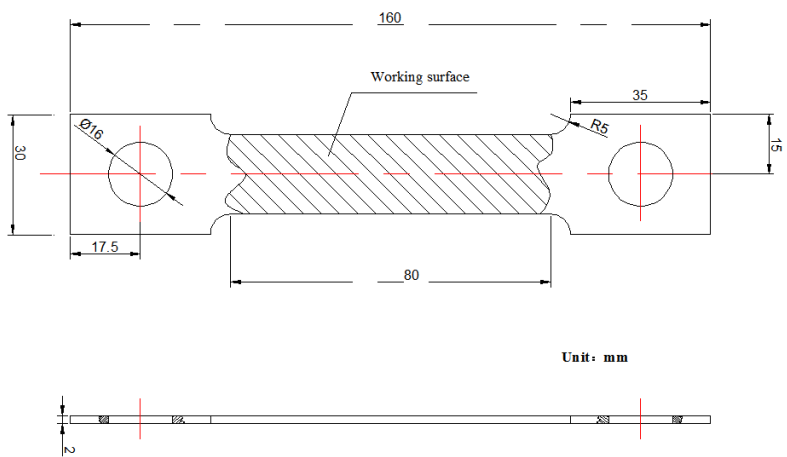


Figure 1. Dimensions of the sample used in the study

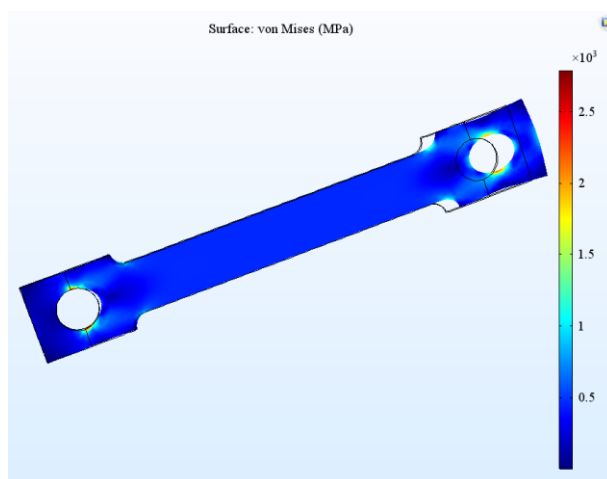


Figure 2. Von Mises stress distribution on the sample surface under the influence of 364 MPa stress

2.2 Electrochemical test method

Fig. 3 shows the schematic of the experimental set-up for electrochemical corrosion test with stray current, using a three-electrode system. The auxiliary electrode was a platinum plate electrode, the reference electrode was a saturated calomel electrode (SCE), and the working electrode was a X70 steel sample with the 3PE coating. The reference electrode was placed in a Lukin capillary tube, with the reference electrode tip 1-2 mm from the sample surface to reduce the influence of the ohmic potential on the potential measurement. Experiments were conducted using PARSTAT2273 instrument and Powersuit software. The SG1005 signal generator was used as the AC power supply to obtain a sinusoidal signal output with a frequency of 50 Hz. WYJ-2A-type dual DC power supply was used as the DC power supply. Firstly, a 5000 μF capacitor was connected to the AC loop to prevent the AC loop from interfering with the DC loop. Then, a 15 H inductor was inserted in the DC loop to prevent the DC signal from interfering with the AC loop. This ensured that the two circuits were independent of one another and did not interfere with each other. The stray current value was regulated through a variable resistor and was read directly from the ammeter. Secondly, AC signals of different densities (0 A/m^2 , 30

A/m², 100 A/m², and 300 A/m²) and DC signals of different densities (0 A/m², 30 A/m², 100 A/m², and 300 A/m²) were generally applied to the circuit during the tests. The current density was calculated based on the damaged area of the coating. The RGM-6050 slow-stress stretcher was used for application of 364 MPa tensile stress. After 24 hours of experimentation, tests for open circuit potential and polarization curve began. It should be noted that when the open circuit potential was stable, test for potentiodynamic polarization curve was performed at room temperature at a scan rate of 0.5 mV/s, and the scanning potential range was from -0.7 V to 0.5 V(V, SCE). Finally, polarization curves were fitted using C-View software.

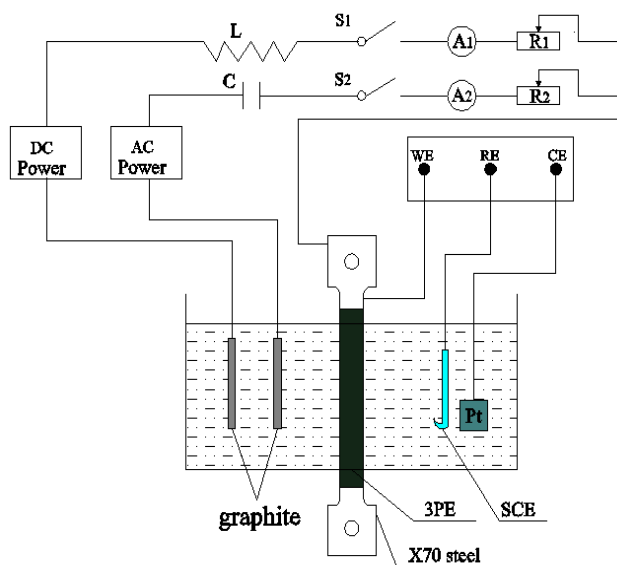


Figure 3. Experimental set-up for stray current corrosion electrochemical test

2.3 Corrosion morphology and measurement of corrosion rate

After the experiment ended, a photograph of the corrosion sample was captured using a digital camera. Then, the anticorrosive layer was scraped and the sample surface was cleaned with Clark's solution. The solution is composed of 1 L hydrochloric acid (specific gravity 1.19), 20 g antimony trioxide (chemical pure reagent), and 50 g stannous oxide (chemical pure reagent). Finally, the sample was rinsed with deionized water and dried using cold air. After the sample was dried in the drying oven, the weight of the sample before and after corrosion was recorded to an accuracy of 0.1 mg using an AB204-E analytical balance. All experiments were repeated twice. To reduce the experimental error, blank uncorroded test pieces of the same sample were treated under the same conditions of pickling. The weight loss method was used to test the corrosion rate, which was calculated using the following formula:

$$\Delta W = W_0 - W_1 - W_2 , \quad V_{\text{corr}} = 1.12 \times \frac{\Delta W}{S t} \quad (1)$$

Where, ΔW is the average weight loss of the sample, g; W_0 is the original weight of the sample, g; W_1 is the mass of the sample after removal of the corrosion products, g; W_2 is the mass loss of the blank sample in the rust removal process, g; t is the soaking time, h; and V_{corr} is the average corrosion rate, mm/a.

The process for removal of rust after the immersion test was the same as that employed for the determination of corrosion rate. After the corrosion products were removed, the corrosion morphology of the X70 steel at the damaged portion of the corrosion layer was studied by three-dimensional microscopy (Keyence VHX-3000).

3. RESULTS AND DISCUSSION

3.1 Open circuit potential results and analysis

Self-corrosion potential is a thermodynamic measure of corrosion occurring in metals. More negative the potential, the more significant is the potential difference between the anode and cathode. In other words, the higher the thermodynamic tendency of the reaction, the higher is the possibility of metal corrosion. Fig. 4 shows the open circuit potentials of the samples measured after soaking for 24 h under the combined influence of AC-DC stray current and stress at 364 MPa. Firstly, as can be seen from Figs. 4(a)-(d), when the applied DC density was constant, the corrosion potential shifted to the negative side as the applied AC density increased. When only the AC interference was applied, the corrosion potential shifted to the negative side from -0.713 V at 0 A/m² to -0.925 V at 300 A/m², and its amplitude was 0.212 V. Secondly, as can be seen from Fig. 4(e), when only the DC interference was applied, as the DC density increased, the corrosion potential shifted negatively from -0.713 V at 0 A/m² to -1.26 V at 300 A/m², which was a shift of 0.547 V. Finally, comparison of Figs. 4(a) and (e) showed that the magnitude of negative shift of corrosion potential caused by DC interference at the same current density was larger than that caused by AC interference. Therefore, AC interference had a more significant influence on the self-corrosion potential of X70 steel, which affected the thermodynamic properties of X70 steel and made it more susceptible to corrosion. A mathematical model of this problem was established [31], which is as follows:

$$E_{corr, AC} = E_{corr} - \left[\frac{b_a}{b_c - 1} \right] \ln \left[\frac{\sum_{k=1}^{\infty} \frac{1}{(k!)^2} \left(\frac{E_p}{2b_c} \right)^{2k} + 1}{\sum_{k=1}^{\infty} \frac{1}{(k!)^2} \left(\frac{E_p}{2b_a} \right)^{2k} + 1} \right] \quad (2)$$

Where, $E_{corr, AC}$ and E_{corr} are corrosion potentials with and without AC interference, respectively, V; b_a and b_c are the Tafel slopes of the anode and the cathode, respectively; and E_p is the peak potential of the applied AC signal, V.

It is evident that the change of corrosion potential caused by AC interference is a function of E_p and the ratio of the anode Tafel slope to the cathode Tafel slope ($r = b_a/b_c$). As E_p increases, the corrosion potential shifts in the negative direction. The offset direction depends on the ratio of the Tafel slopes of the anode and cathode, that is, only if $r \neq 1$, AC will corrode the metal. In case of a fixed surface defect area, the AC density is proportional to E_p , so the corrosion potential shifts negatively as AC density

increases. According to thermodynamics, under the action of AC-DC stray current either alone or together, with an increase in current density, the corrosion potential of X70 steel shows negative shift. This is conducive for oxidation reaction and makes X70 steel more susceptible to corrosion, which is consistent with the conclusions drawn by Zhang [32].

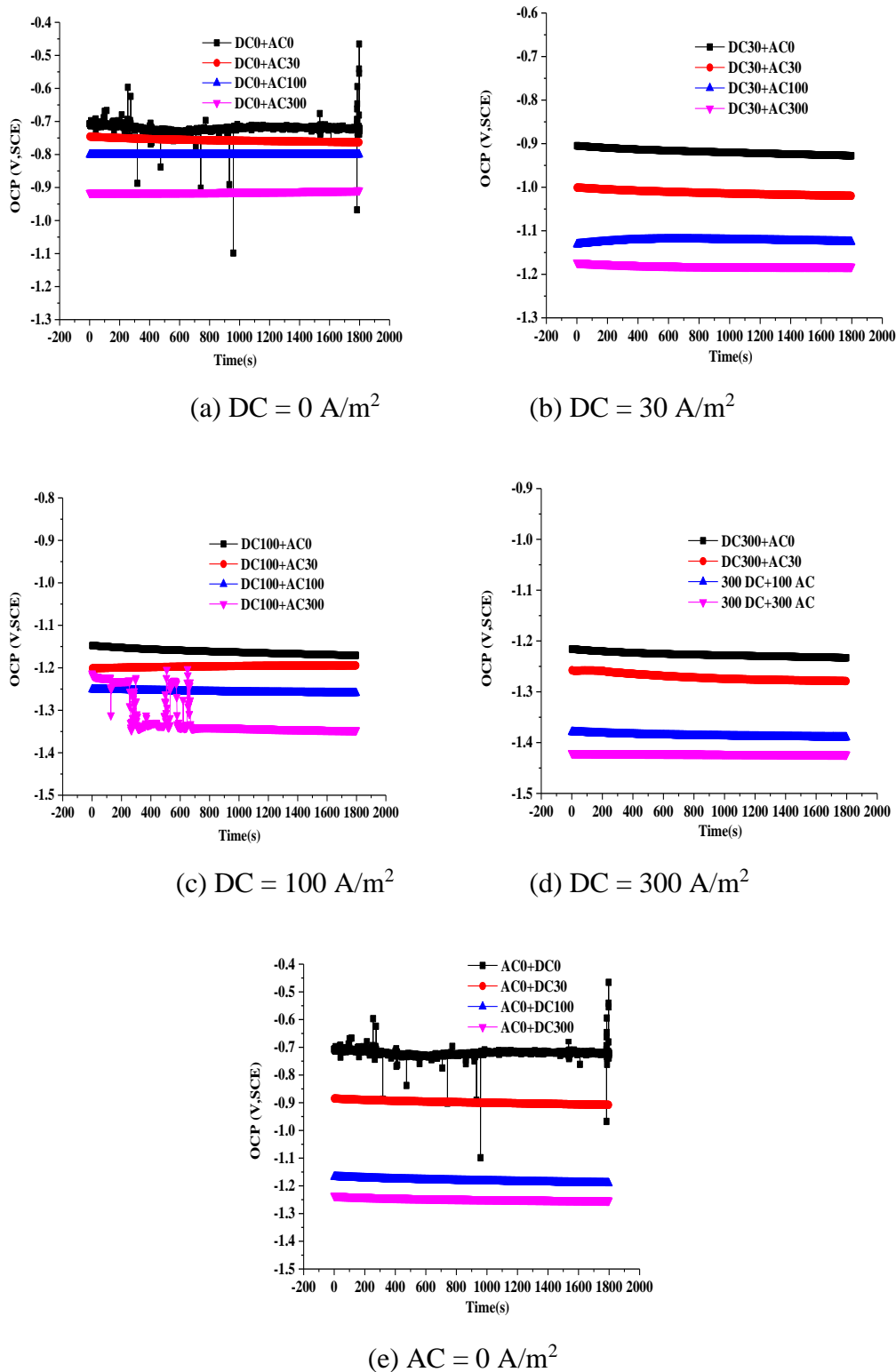


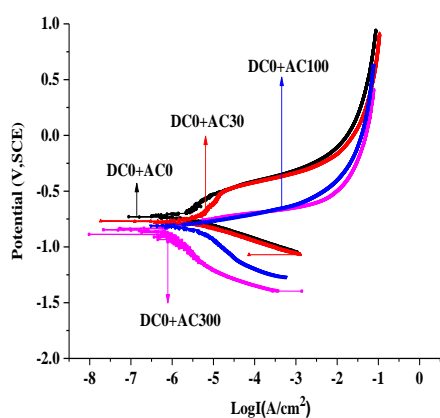
Figure 4. Open circuit potentials under the combined action of 364 MPa stress and AC-DC stray current

3.2 Results and analysis of polarization curves

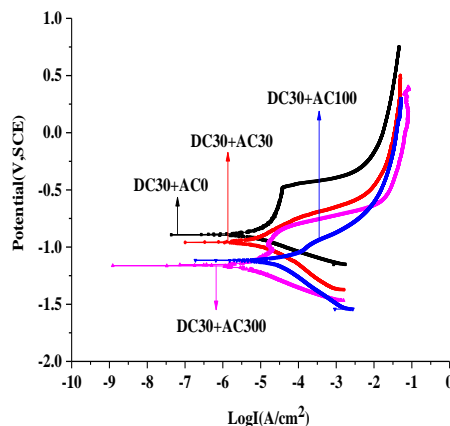
The polarization curves of the samples due to the combined action of 364 MPa stress and AC-DC stray current are shown in Fig. 5. It can be seen that the anodic polarization curve was smoother in presence of only AC interference. However, in presence of DC interference, the anodic polarization curve showed an obvious inflection point, which could be due to a large number of corrosion products that covered the defects of the coating layer and affected the anodic polarization process. With an increase in the anodic polarization potential, the anodic polarization curve became steeper and the corrosion current increased continuously. X70 steel was still in the active dissolution state without passivation. When the applied DC density was constant, as the AC density increased, the corrosion potential shifted to the negative side and the anode current density increased rapidly. Results from the polarization curve confirmed that the presence of stray currents affected the corrosion process of the X70 steel. The application of AC-DC interference was not conducive for the formation of a passive film on the surface of X70 steel. The result was that X70 steel showed no passivation tendency in the test system. Also, the higher the current density, the greater is the anode current density, and more is the dissolution tendency of X70 steel. The influence of the AC-DC stray current on the Tafel constant was significant. When stray current was applied, the Tafel constants of both the anode and cathode changed significantly, and the effect of AC-DC interference on the anodic polarization process of X70 steel was obviously greater than that on cathode polarization process.

According to the Tafel extrapolation principle, Tafel slope, self-corrosion current density, and other parameters can be fitted. The self-corrosion current parameters fitted by polarization curves of samples, subjected to combined AC-DC interference at different current densities and stress of 364 MPa, are shown in Fig. 6. Fig 7 shows the corrosion rates determined by the weight loss method for the combined influences of different AC-DC densities and stress of 364 MPa. The figure shows that the corrosion rates calculated by the Tafel extrapolation method and those obtained by the weight loss method were different, but the trends were consistent. This implied that when the applied DC density was constant, the corrosion current and the corrosion rate increased gradually with increase in AC density. When the applied AC density was constant, as the DC density increased, the corrosion current, and the corrosion rate increased. The corrosion current of samples under the collective action of AC-DC stray currents was higher than that under the individual action of AC or DC interference. When only AC interference was applied, the corrosion current and corrosion rate were relatively small. However, they increased significantly when the DC interference was introduced into this system. The corrosion rate in presence of DC interference was obviously higher than that in presence of AC interference at the same current density. The corrosion current was 5.68×10^{-4} A/cm², and the corrosion rate was 1.2 mm/a in the presence of a DC interference of 300 A/m² alone. However, the corrosion current was 1.34×10^{-5} A/cm², and the corrosion rate was 0.48 mm/a in the presence of AC interference of 300 A/m² alone. This showed that the amount of corrosion caused by an equal amount of DC interference was more significant than that of AC interference. This could be attributed to the fact that most of the AC interference became a non-identical current puller and generated a discharge phenomenon, when it passed through an electric double layer capacitor. Only a small amount of AC interference was involved in the corrosion processes

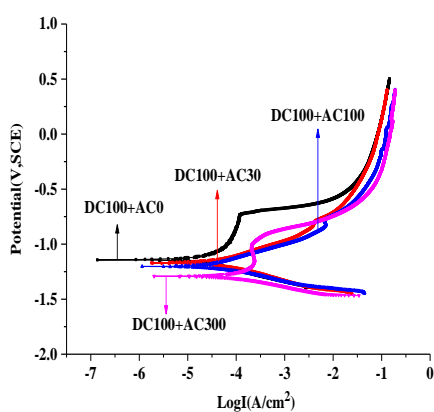
of charge transfer as the Faraday current [33]. These results are consistent with the results of polarization curve fitting.



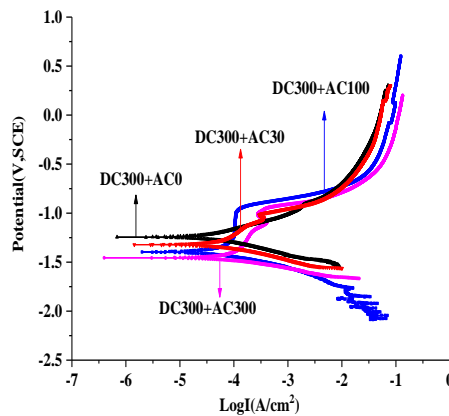
(a) DC = 0 A/m²



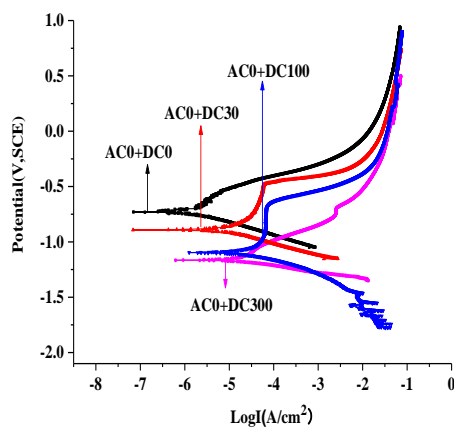
(b) DC = 30 A/m²



(c) DC = 100 A/m²



(d) DC = 300 A/m²



(e) AC = 0 A/m²

Figure 5. Polarization curves of the sample measured under the combined action of 364 MPa stress and AC-DC interference

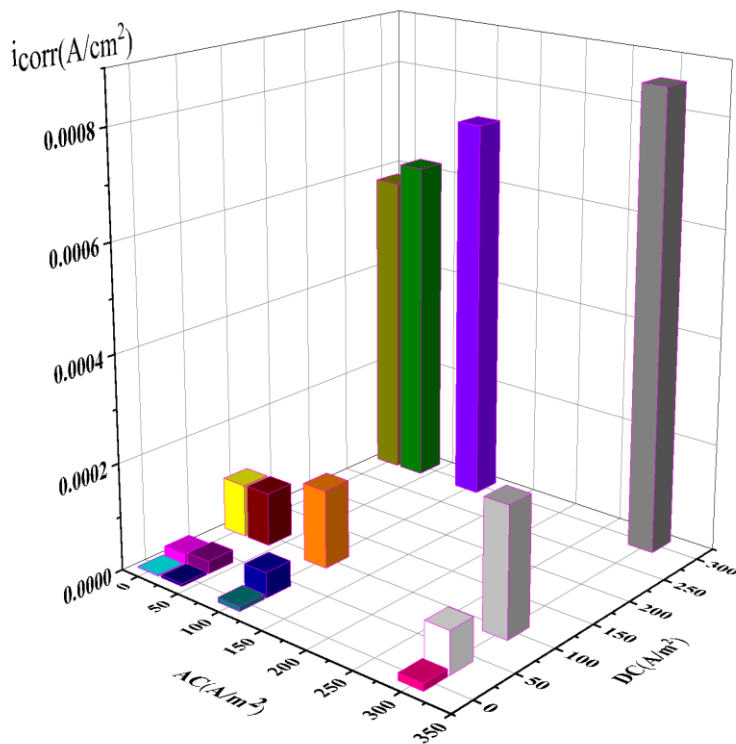


Figure 6. The corrosion current parameters fitted by the polarization curve under the combined action of 364 MPa stress and AC-DC interference at different current densities: (a) 0 A/m^2 , (b) 30 A/m^2 , (c) 100 A/m^2 , and (d) 300 A/m^2

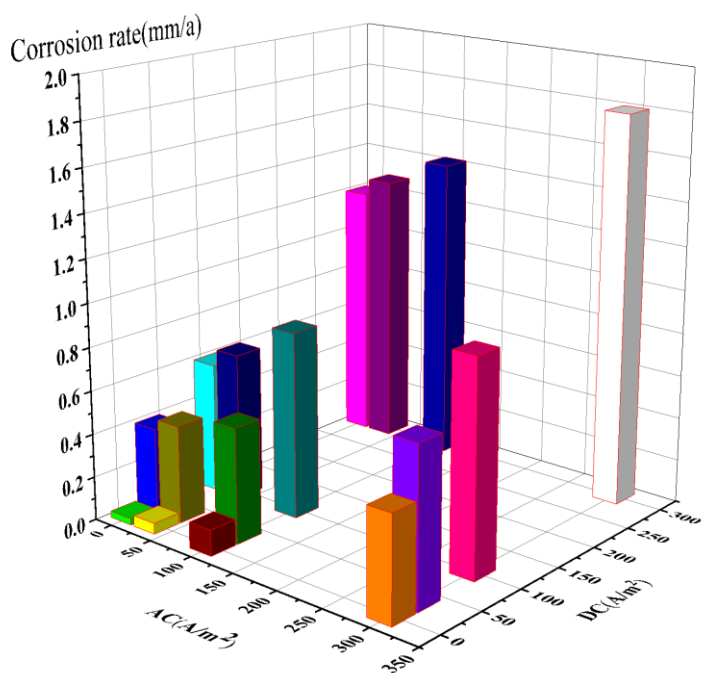
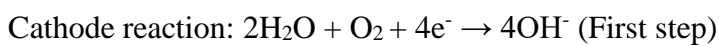
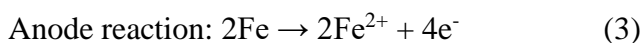


Figure 7. Corrosion rate determined by the weight loss method under the combined action of 364 MPa stress and AC-DC interference at different current densities: (a) 0 A/m^2 , (b) 30 A/m^2 , (c) 100 A/m^2 , and (d) 300 A/m^2

3.3 Corrosion morphological analysis

Figs. 8~11 show the corrosion morphologies of samples under the combined actions of 364 MPa stress and AC-DC interference at different densities. Fig. 12 shows the etch pit depths of the samples under the same conditions. From the figure, it was evident that at a constant applied DC density, the maximum corrosion pit depth on the X70 steel at the defect site of the coating increased gradually as the AC density increased. Additionally, when the applied AC density was constant, the maximum pit depth increased as the DC density increased. The depth of corrosion pit under the influence of AC-DC stray current was more than that under the individual actions of either AC or DC interference. The corrosion pit appeared shallow when only AC interference was applied, whereas it increased significantly when DC interference was applied. The corrosion pit depth under the influence of DC interference was obviously more than that under the influence of AC interference at the same current density. The pit depth was 503 μm when DC interference of 300 A/m^2 was applied individually, while it was 224 μm when AC interference of 300 A/m^2 was applied individually. These results were similar to those obtained by the weight loss method. Also, a large number of small, colorless, and odorless bubbles were seen on the surface of the X70 steel samples in the later stages of corrosion under the influence of the AC-DC interference, indicating that a hydrogen reduction reaction occurred:



In the anodic reaction, the surface of the sample was oxidized. In the first stage of the cathodic reaction, there was sufficient amount of oxygen in the solution to generate OH^- . In the later phases of cathodic reaction, OH^- and H_2 were generated due to the lack of oxygen in the solution. The OH^- product combined with the anodic reaction products to form a corrosion film as the final product. The corrosion rate of metal due to AC interference was determined by the solubility of the anode and was related to the anode current density. The amount of metal corroded by DC interference obeyed the electrolytic law, that is, Faraday's law, according to which, the amount of corroded material produced is proportional to the amount of current passed [17]. Xu [34] studied the influence of AC on the corrosion of buried pipelines in Shengli Oilfield using polarization curves and weight loss methods. Results showed that with increasing AC density (0~400 A/m^2), the corrosion rate gradually increased and the maximum depth of the pit increased gradually. Yu [35] studied the corrosion effects of DC interference on Q235 steel in Yingtan soil environment. Studies have shown that with increase in DC density, maximum depth of corrosion pit on the sample surface increased gradually. Wen [36] showed that the corrosion rate increased with increase in stray current density. AC interference was found to be less corrosive than DC interference. The combined influence of AC-DC stray current showed greater corrosion rate than the corrosion rate of AC or DC individually. The results of this study were found to be consistent with the findings of the above mentioned scholars [34-36].

Fig. 13 shows the delamination areas of samples under the combined influence of both, 364 MPa stress and AC-DC interference, at different current densities. It could be seen that under the influence of AC interference alone, the delamination area of the coating increased from 1.2 mm² at 0 A/m² to 4.2 mm² at 100 A/m². Thereafter, as the AC density increased continuously up to 300 A/m², the delamination area did not show any significant changes. This is due to the accumulation of corrosion products in the region where the coating was damaged. This caused blockage of the corrosion channel and the electron exchange between the cathode and the anode became relatively difficult. At the same time, due to decrease in oxygen content of the solution, the effect of AC interference on delamination was significantly weakened.

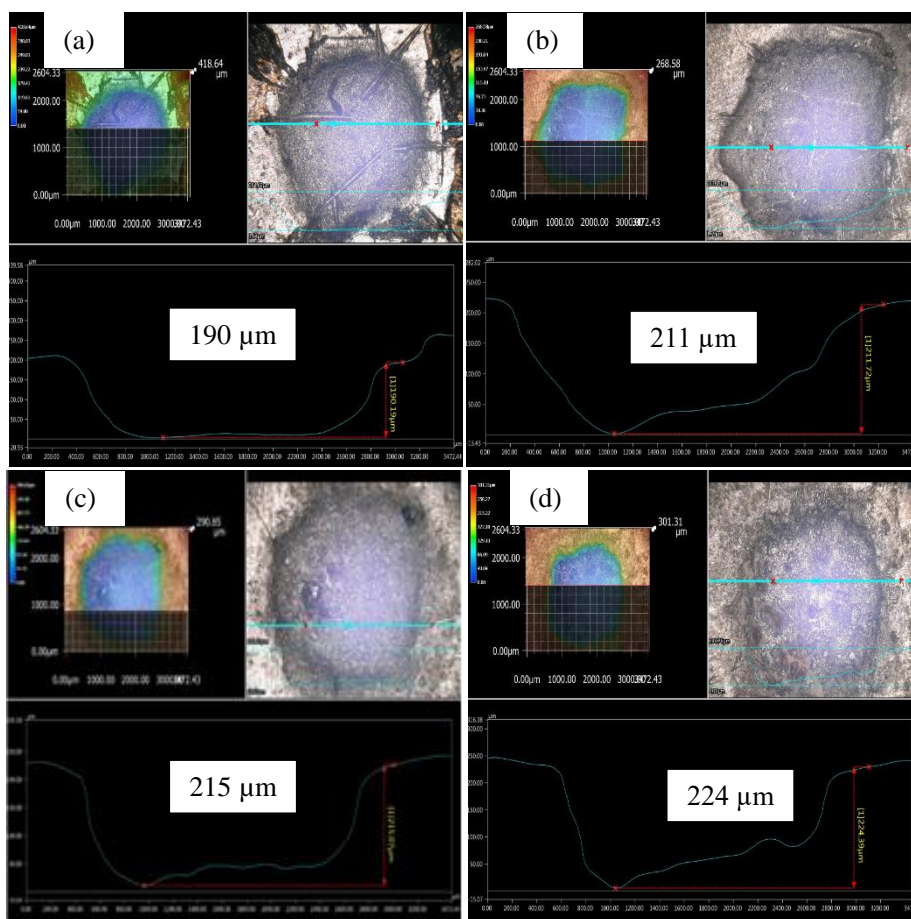


Figure 8. Corrosion morphologies of samples under the conditions of 364 MPa stress and different AC densities: (a) 0 A/m², (b) 30 A/m², (c) 100 A/m², and (d) 300 A/m²

In the presence of DC interference alone, the delamination area increased gradually with increase in current density. When the applied DC density was constant, the delamination area of the coating increased slightly with increase in the AC density. However, when the applied AC density was constant, it increased obviously with increase in AC density. The combined effects of AC-DC stray currents resulted in a larger delamination area compared to that caused by the action of AC or DC interference individually. The results of this study suggested that DC interference had greater impact on the

delamination compared to that of AC interference. Fig. 14 is a schematic view of the delamination process of an anti-corrosion layer under the combined influence of stray current and stress. It can be seen from the figure that the corroded film formed in the corrosion reaction prevented oxygen from penetrating into the defects below the corroded film, resulting in an oxygen-depleted region below the film at the center of the defect. However, oxygen could diffuse through the edge of the corroded film to the defective edge, which made the defective edge an oxygen-rich area and formed separate anode and cathode regions. Due to the low pH of the anode region, the dissolution of the metal at the anode was accelerated. The pH of cathode region was higher, which reduced the adhesiveness of the anti-corrosion layer due to the formation of OH^- and H_2 . The coating lost its tackiness due to saponification reaction, which led to the cathodic delamination of the coating [37].

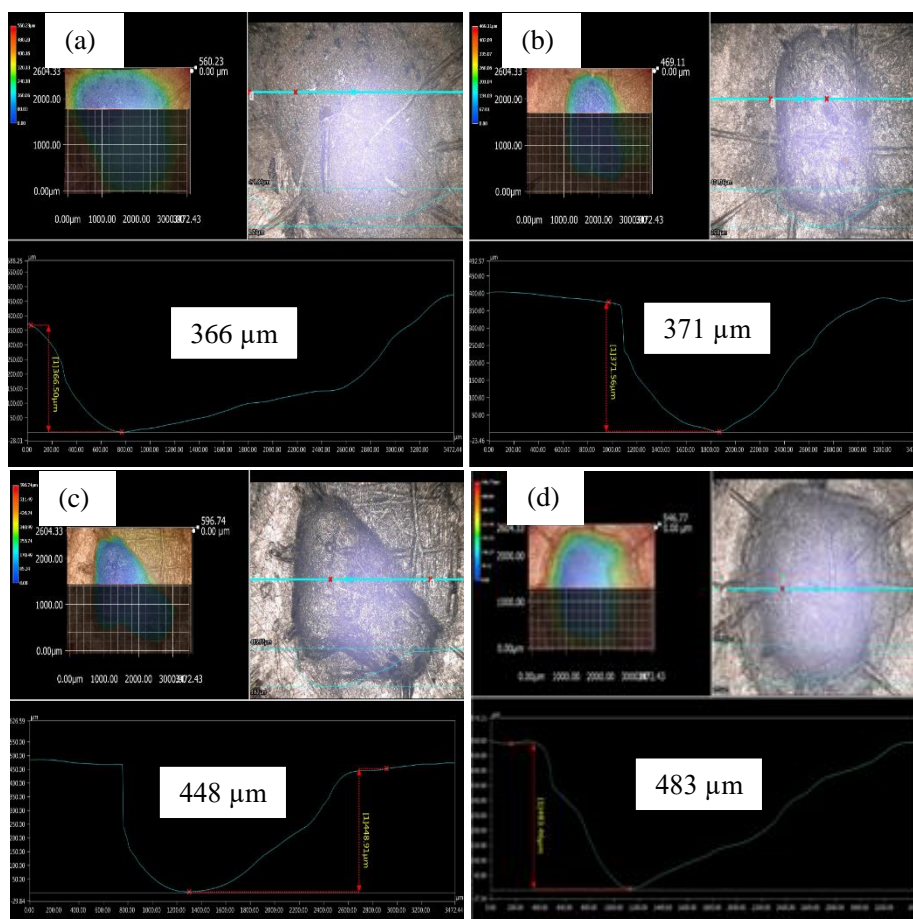


Figure 9. Corrosion morphologies of samples under the conditions of 364 MPa stress, DC density of 30 A/m^2 , and different AC densities: (a) 0 A/m^2 , (b) 30 A/m^2 , (c) 100 A/m^2 , and (d) 300 A/m^2

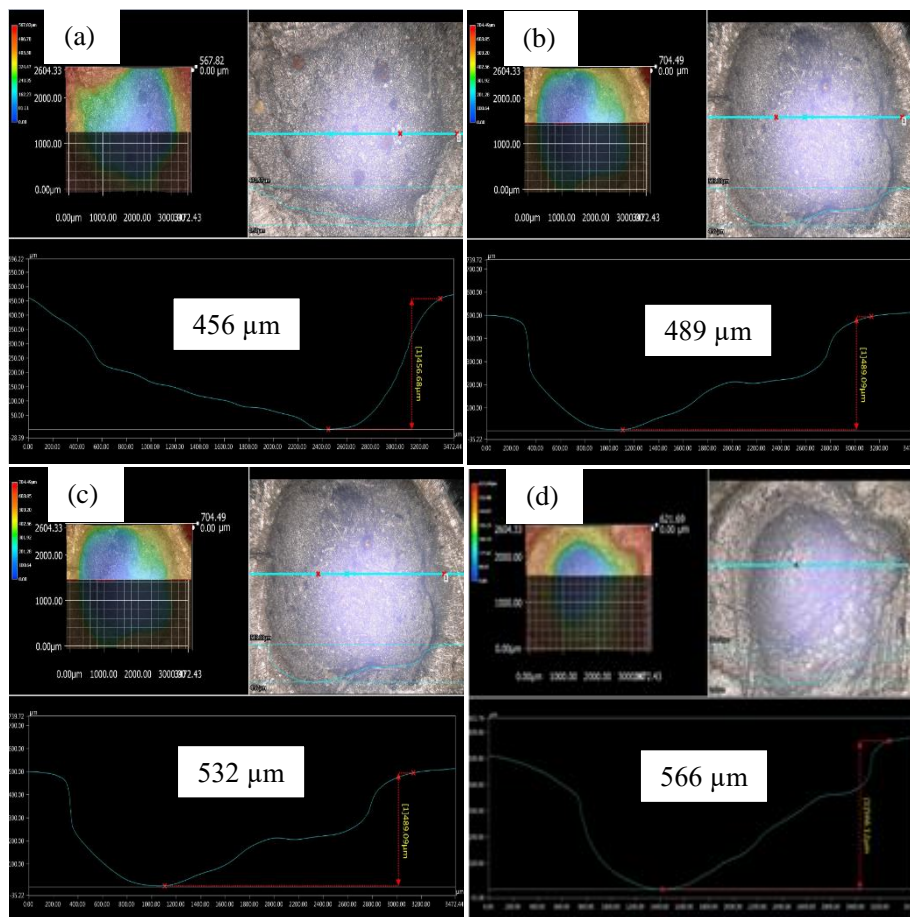


Figure 10. Corrosion morphologies of samples under the conditions of 364 MPa stress, DC densities of 100 A/m², and different AC densities: (a) 0 A/m², (b) 30 A/m², (c) 100 A/m², and (d) 300 A/m²

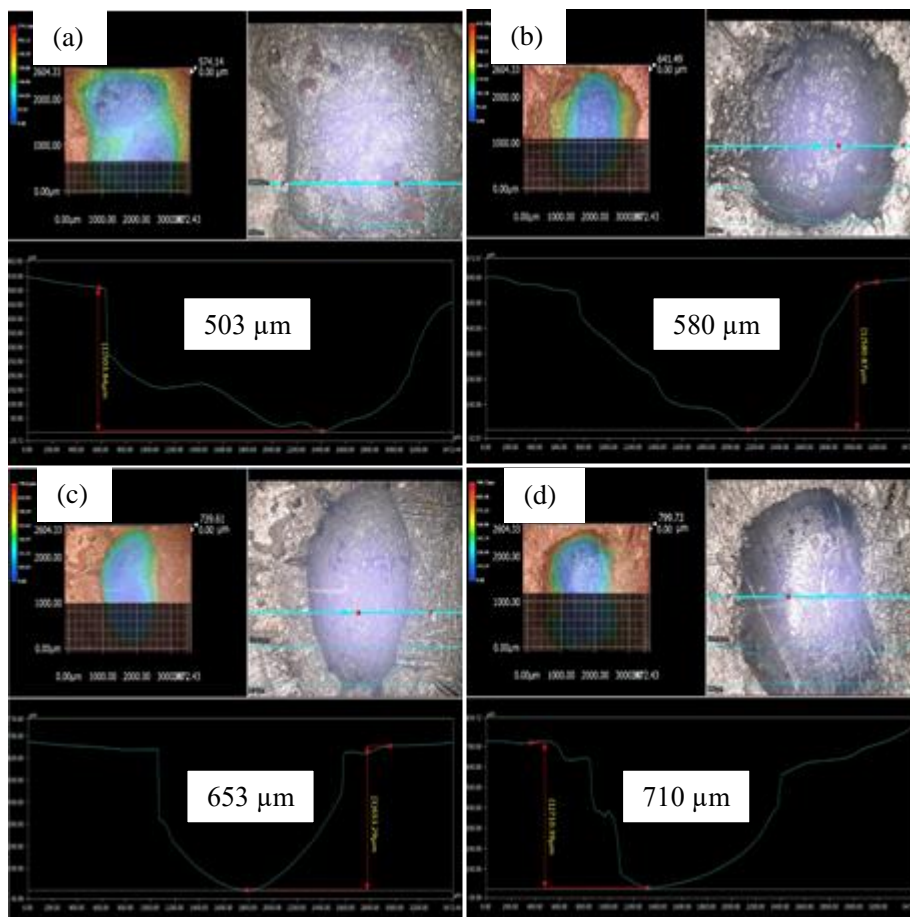


Figure 11. Corrosion morphologies of samples under 364 MPa stress, DC densities of 300 A/m², and different AC densities: (a) 0 A/m², (b) 30 A/m², (c) 100 A/m², and (d) 300 A/m²

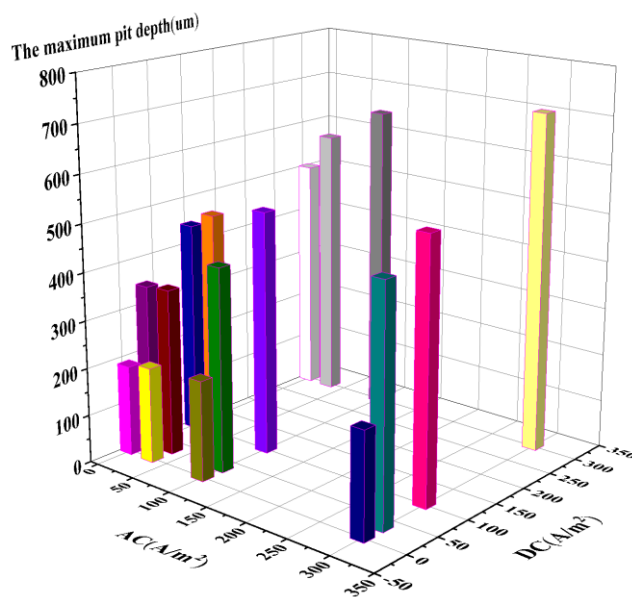


Figure 12. Maximum pit depths of samples under the conditions of 364 MPa stress and different AC-DC densities: (a) 0 A/m², (b) 30 A/m², (c) 100 A/m², and (d) 300 A/m²

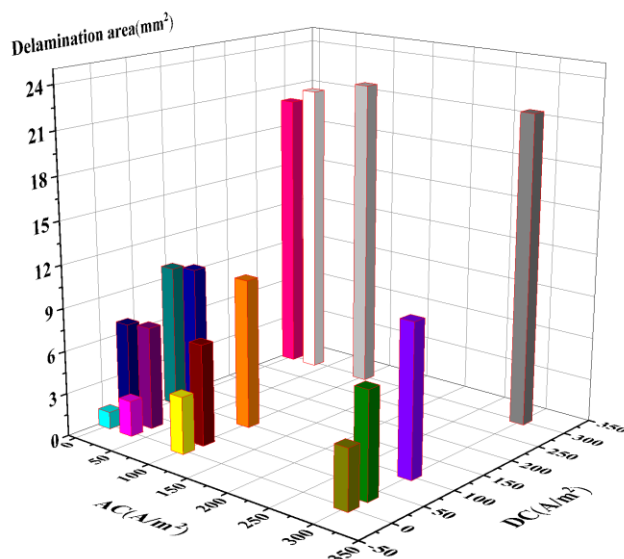


Figure 13. Delamination areas of samples under the conditions of 364 MPa stress and different AC-DC densities: (a) 0 A/m², (b) 30 A/m², (c) 100 A/m², and (d) 300 A/m²

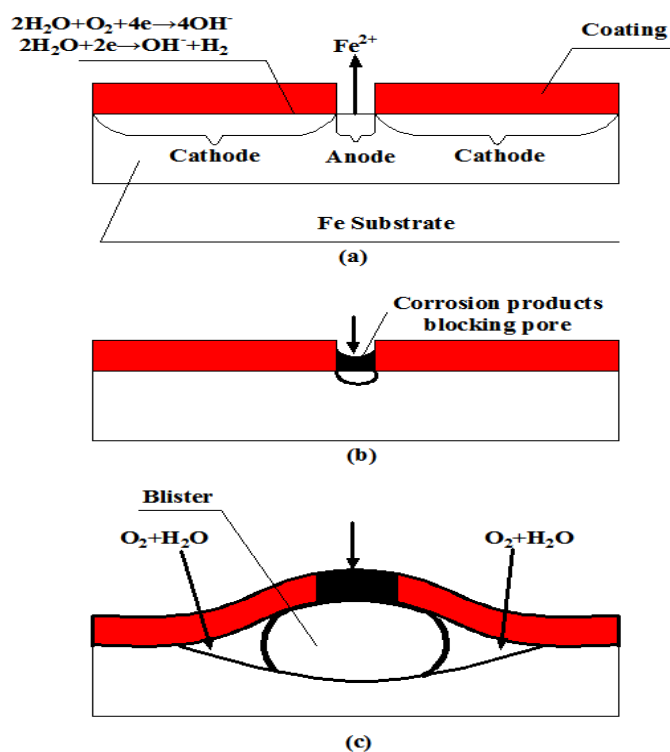


Figure 14. Schematic diagram of the delamination process at the site of coating defect under the combined influence of stray current and stress

4. CONCLUSIONS

(1) Under the influence of 364 MPa stress, with increase in stray current density, the corrosion potential shifted to the negative side. The magnitude of the negative shift of corrosion potential caused

by DC was larger than that caused by AC. Polarization curves showed only active dissolution zones and no passivation zones. The anodic polarization curve gradually became steeper as the current density increased. Under the influence of DC interference, the anodic polarization curve showed a sharp inflection point, due to the accumulation of large number of corrosion products on the surface of X70 steel sample, which temporarily hindered the anodic polarization process.

(2) The corrosion rate measured by the weight loss method was consistent with the results of the polarization curve fitting. Accordingly, as the stray current density increased, the corrosion rate increased gradually, following Faraday's law of electrolysis. Under the same conditions, the corrosion rates were in the following order: combined AC and DC interferences > DC interference > AC interference.

(3) Observation of the corrosion specimen under a three-dimensional bulk microscope showed that the depth of corrosion pit on the specimen surface increased as the current density increased. Under the same conditions, the depths of the corrosion pits were in the following order: combined AC and DC interferences > DC interference > AC interference.

(4) The effect of AC interference on the delamination was smaller than that of the DC interference. The delamination area under the influence of DC interference with a density of 300 A/m² was approximately 5 times that under the influence of AC interference. The delamination area under the combined influence of AC-DC stray currents was greater than that under the influence of either AC or DC individually. The model of delamination process under the action of stray currents was proposed. According to it, corrosion at the coating defects occurred first. When the corrosion products accumulated to a certain extent, separate cathode and anode regions were formed on the surfaces of the samples at the defects, and this resulted in delamination.

ACKNOWLEDGEMENTS

This work was supported by National Natural Science Foundation of China (No. 51471011) and "Rixin Scientist" of Beijing University of Technology.

References

1. A. L. Cao, Q. J. Zhu, S. T. Zhang and B. R. Hou, *Anti-Corros Method M.*, 57 (5) 234.
2. S. R. Allahkaram, M. Isakhani-Zakaria and M. Derakhshani, *J. Nat. Gas Sci. Eng.*, 26 (2015) 453.
3. A. O. S. Solgaard, M. Carsana and M. R. Geiker, *Corros. Sci.*, 74 (2013) 1.
4. Z. G. Chen, C. K. Qin, J. X. Tang and Y. Zhou, *J. Nat. Gas Sci. Eng.*, 15 (2013) 76.
5. L. Sandrolini, *Electr Pow Syst Res*, 103 (2013) 248.
6. A. Dolara, F. Foiadelli and S. Leva, *IEEE Trans. Power Deliv.*, 27 (2012) 2304.
7. C. A. Charalambous, I. Cotton, P. Aylott and N. D. Kokkinos, *IEEE Trans. Power Deliv.*, 28 (2013) 1048.
8. R. Floyd, Testing and Mitigation of AC Corrosion on 8 Line: A Field Study, Proc. of Nace International Conference Corrosion, New Orleans, Louisiana, 2004, Page No.04210.
9. H. R. Hanson and J. Smart, AC Corrosion on a Pipeline Located in a HVAC Utility Corridor, NACE International Conference Corrosion, New Orleans, Louisiana, 2004, Page No.04209.
10. M. Yan, S. Yang and J. Xu, *Acta Metall. Sin.*, 52 (2016) 1133.
11. J. Zhao, F Xie and K Gong, *Surf. Technol.*, 46 (2017) 108.

12. G. X. Zhong, Q. Shi and Q. K. Zhao, *Surf. Technol.*, 45 (2016) 106.
13. K. Huang, J. L. Wu and K. Quan, *Surf. Technol.*, 47 (2018) 116.
14. Z. S. Li, Z. Y. Liu and C. W. Du, *Surf. Technol.*, 45 (2016) 1.
15. X. Li, Q. J. Zhu and N. Zhu, *Surf. Technol.*, 46 (2017) 206.
16. A. Ogunsola, A. Mariscotti and L. Sandrolini, *IEEE Trans. Power Deliv.*, 27 (2012) 2238.
17. L. Bertolini, M. Carsana and P. Pedferri, *Corros. Sci.*, 49 (2007) 1056.
18. X. Wang, X. Tang and L. Wang, *J. Nat. Gas Sci. Eng.*, 21 (2014) 474.
19. H Song, Y kim and P Yong, Competition of AC and DC Current in AC Corrosion Under Cathodic Protection, NACE International Conference Corrosion, Denver, Colorado, 2002, Page No.02117.
20. S. Goidanich, L. Lazzari and M. Ormellese, *Corros. Sci.*, 52 (2010) 916.
21. A. Fu and Y. Cheng, *Corros. Sci.*, 52 (2010) 612.
22. Y. B. Guo, T. Meng and D. G. Wang, *Eng Fail Anal.*, 78 (2017) 87.
23. X. Wang, C. Xu and Q. Liu, *Int. J. Electrochem. Sci.*, 12 (2017) 6520.
24. F. E. Kulman, *Corrosion*, 17 (1961) 34.
25. U. Bertocci, *Corrosion*, 35 (1979) 1281.
26. D. A. Jones, *Corrosion*, 34 (1978) 428.
27. L. Lazzari, S. Goidanich and M. Pedferri and M. Ormellese, Influence of AC on corrosion kinetics for carbon steel, zinc and copper, Corrosion 2005, Paper No. 05189.
28. L. Nielsen and F. Galsgaard, Sensor Technology for On-Line Monitoring of AC Induced Corrosion Along Pipelines, Corrosion 2005, Houston, Texas, NACE, No: 05375.
29. Z. Panossian, S. Filho and N. D. Almedida, Effect of alternating current by high power lines voltage and electric transmission systems in pipelines corrosion, Corrosion 2009, Atlanta, NACE, No: 09541.
30. R. K. Ren, S. Zhang and X. L.Pang, *Electrochim. Acta*, 85 (2012) 283.
31. S. B. Lalvani and X. A. Lin, *Corros. Sci.*, 36 (1994) 1039.
32. R. Zhang, P. R. Vairavanathan and S. B. Lalvani, *Corros. Sci.*, 50 (2008) 1664.
33. T. J. Lennox and M. H. Peterson, *Nav. Eng. J.*, 88 (2010) 45.
34. L. Y. Xu, X. Su, Z. X. Yin, Y. H. Tang and Y. F. Cheng, *Corros. Sci.*, 61 (2012) 215.
35. J. F. Yu and M. Zhang, *Mater. Prot.*, 48 (2015) 14.
36. C. Wen, J. Li, S. Wang and Y. Yang, *J. Nat. Gas Sci. Eng.*, 27 (2015) 1555.
37. D. Weijde, E. Westing and J. Wit, *Electrochim. Acta*, 41 (1996) 1103.